Multiple risk pathways for schizophrenia converge in serine racemase knockout mice, a mouse model of NMDA receptor hypofunction

Darrick T. Balu[a,b], Yan Li[a], Matthew D. Puhl[a,b], Michael A. Benneyworth[a,b], Alo C. Basu[a,b], Shunsuke Takagi[c], Vadim Y. Bolshakov[a], and Joseph T. Coyle[a,b,1]

[a]Department of Psychiatry, Harvard Medical School, Boston, MA 02115; [b]Laboratory for Psychiatric and Molecular Neuroscience, Department of Psychiatry, McLean Hospital, Belmont, MA 02478; and [c]Department of Psychiatry and Behavioral Sciences, Graduate School of Medical and Dental Sciences, Tokyo Medical and Dental University, Bunkyo-ku, Tokyo 113-8519, Japan

Edited* by Solomon H. Snyder, The Johns Hopkins University School of Medicine, Baltimore, MD, and approved May 7, 2013 (received for review March 5, 2013)

Schizophrenia is characterized by reduced hippocampal volume, decreased dendritic spine density, altered neuroplasticity signaling pathways, and cognitive deficits associated with impaired hippocampal function. We sought to determine whether this diverse pathology could be linked to NMDA receptor (NMDAR) hypofunction, and thus used the serine racemase-null mutant mouse ($SR^{-/-}$), which has less than 10% of normal brain D-serine, an NMDAR coagonist. We found that D-serine was necessary for the maintenance of long-term potentiation in the adult hippocampal dentate gyrus and for full NMDAR activity on granule cells. $SR^{-/-}$ mice had reduced dendritic spines and hippocampal volume. These morphological changes were paralleled by diminished BDNF/Akt/mammalian target of rapamycin (mTOR) signaling and impaired performance on a trace-conditioning memory task. Chronic D-serine treatment normalized the electrophysiological, neurochemical, and cognitive deficits in $SR^{-/-}$ mice. These results demonstrate that NMDAR hypofunction can reproduce the numerous hippocampal deficits associated with schizophrenia, which can be reversed by chronic peripheral D-serine treatment.

miR-132 | MeCP2 | glycogen synthase 3 kinase | CREB

Schizophrenia is a severe psychiatric disorder that affects 1% of the population worldwide (1). There are widespread morphological, neurochemical, and functional changes in the brain in schizophrenia that have been linked to its symptomatic features (2). For example, the hippocampus of patients with schizophrenia exhibits reduced dendritic spine density (3), atrophy (4), and impaired activation while performing cognitive tasks (5). The neuroplasticity deficits observed in schizophrenia could be caused by a constellation of factors.

Impaired neurotrophic signaling could be one mechanism underlying these abnormalities. BDNF regulates a complex array of processes, including neurite outgrowth and spine density, by signaling through tropomyosin receptor kinase B (TrkB), its high-affinity receptor (6). In postmortem studies, BDNF mRNA and protein (7–9) levels, as well as TrkB mRNA (7, 10, 11) and protein (12), are reduced in subjects with schizophrenia. V-akt murine thymoma viral oncogene (Akt) is a kinase downstream of TrkB. Not only is the Akt1 isoform a putative schizophrenia risk gene (13), its expression (14, 15) and the amount of phosphorylated Akt (p-Akt) (16) in the dentate gyrus (DG) are reduced in schizophrenia.

Aberrant microRNA (miR) processing might also be contributing to the pathophysiology of schizophrenia (17). These noncoding RNAs regulate neural plasticity by controlling the translation of target mRNA transcripts. Expression of the neuron-enriched miR-132 is reduced in schizophrenia (18); it regulates basal and activity-induced neurite outgrowth (19), and is up-regulated in vivo in response to external stimuli (20, 21). Importantly, both BDNF (22) and miR-132 (17) expression are increased by NMDAR receptor (NMDAR) activation.

Pharmacologic and biochemical evidence has converged to support NMDAR hypofunction as a key etiological component of schizophrenia (23–26). Furthermore, meta-analysis of genetic association studies (27) and recent large-scale, copy number variants analyses (28, 29) have implicated the NMDAR and proteins associated with the postsynaptic density in the etiology of schizophrenia. NMDAR activation requires postsynaptic depolarization, binding of glutamate, and binding of either glycine or D-serine at the glycine modulatory site (GMS). D-serine is enriched in corticolimbic regions of the brain, where its localization closely parallels that of NMDARs (30). Genetic and biochemical findings suggest that serine racemase (SR), the enzyme that converts L-serine to D-serine, and D-serine itself are reduced in schizophrenia (31–35).

Therefore, our laboratory generated a mutant mouse in which exon 1 of the SR gene was constitutively deleted (36). SR deletion produces a 90% reduction in cortical D-serine, resulting in NMDAR hypofunction (36). In the present study, we characterize how NMDAR hypofunction in SR knockout ($SR^{-/-}$) mice affects numerous aspects of adult hippocampal neuroplasticity and behavior, and demonstrate that these deficits can be reversed with chronic D-serine treatment.

Significance

We sought to determine whether the diverse hippocampal neuropathology observed in schizophrenia could be recapitulated in an animal model of NMDA receptor (NMDAR) hypofunction. Serine racemase-deficient ($SR^{-/-}$) mice, which lack one of the NMDAR coagonists D-serine, display impaired hippocampal plasticity, as well as the morphological, neurochemical, and cognitive abnormalities consistent with what is observed in schizophrenia. Importantly, treatment in adulthood with D-serine reversed the electrophysiological, neurochemical, and cognitive deficits. These results demonstrate that NMDAR hypofunction can reproduce the hippocampal deficits associated with schizophrenia and point to potential interventions for the currently untreatable negative and cognitive symptoms of this disorder.

Author contributions: D.T.B., Y.L., M.D.P., M.A.B., A.C.B., V.Y.B., and J.T.C. designed research; D.T.B., Y.L., M.D.P., M.A.B., and S.T. performed research; D.T.B., Y.L., and M.D.P. analyzed data; and D.T.B., Y.L., M.D.P., V.Y.B., and J.T.C. wrote the paper.

Conflict of interest statement: J.T.C. is a consultant for Biovail, Puretech, Abbott, and Bristol-Myers Squibb, and owns stock in Abbott. A patent owned by Massachusetts General Hospital for the use of D-serine as a treatment for serious mental illness could yield royalties for J.T.C..

*This Direct Submission article had a prearranged editor.

[1]To whom correspondence should be addressed. E-mail: joseph_coyle@hms.harvard.edu.

This article contains supporting information online at www.pnas.org/lookup/suppl/doi:10.1073/pnas.1304308110/-/DCSupplemental.

Results

NMDAR-Mediated Miniature Excitatory Postsynaptic Current Amplitude Is Decreased in DG Granule Cells of $SR^{-/-}$ Mice. To evaluate the contribution of endogenous D-serine to the activation of NMDARs in the DG, we assessed the parameters of miniature excitatory postsynaptic currents (mEPSCs) recorded from granule cells in control and $SR^{-/-}$ mice. We targeted cells located in the outer third of the granule cell layer to avoid recording from cells at different stages of maturity as a result of adult hippocampal neurogenesis (37). Recorded neurons showed no differences in their input resistance between the groups (four WT mice: 258.9 ± 35.8 MΩ, $n = 11$ cells; four $SR^{-/-}$ mice: 232.6 ± 21.9 MΩ, $n = 11$ cells, $P = 0.27$), indicating that deletion of SR had no effect on the membrane properties of granule cells. The NMDAR-mediated currents (NMDAR mEPSCs) were recorded at a holding potential of –70 mV in the external medium without added Mg^{2+}, and measured at 10 ms after the peak of averaged mEPSCs, which was determined by activation of AMPA receptors (AMPARs). We found that the amplitude of NMDAR mEPSCs was significantly smaller in slices from $SR^{-/-}$ mice (Fig. 1 *B* and *C*) ($P < 0.05$), but the decay time was faster in $SR^{-/-}$ animals (Fig. 1 *E* and *F*) ($P < 0.05$). Exogenously applied D-serine (10 μM) potentiated the amplitude and prolonged the decay time of NMDAR mEPSCs in both WT ($P < 0.05$ for both amplitude and decay time) and $SR^{-/-}$ mice ($P = 0.006$ for amplitude, $P < 0.05$ for decay time), confirming the lack of NMDAR GMS saturation under conditions of basal synaptic transmission (38). In the presence of exogenously applied D-serine, the difference in the amplitude and decay time of NMDAR mEPSCs observed under control conditions was abolished, indicating that the functional properties of the NMDARs in DG granule cells were unaffected in $SR^{-/-}$ mice (39, 40). WT and $SR^{-/-}$ mice did not differ in the amplitude of AMPAR mEPSCs, measured at the peak mEPSC amplitude in the presence of the NMDAR antagonist D-AP5 (50 μM) (Fig. 1 *D* and *G*).

Magnitude of Long-Term Potentiation at the Medial Perforant Pathway to DG Synapses Is Diminished in $SR^{-/-}$ Mice. To test whether NMDAR hypofunction detected in $SR^{-/-}$ mice might impact basal neurotransmission or NMDAR-dependent synaptic plasticity, we stimulated the medial perforant pathway (mPP) and recorded field excitatory postsynaptic potentials (fEPSPs) in the middle molecular layer DG of the hippocampus in slices from WT and $SR^{-/-}$ mice and assessed baseline neurotransmission and high-frequency stimulation-induced long-term synaptic potentiation (LTP). Baseline synaptic transmission, assayed with input-output curves (Fig. 2 *A* and *B*) [genotype: $F(1, 133) = 0.51$, $P = 0.48$] and paired pulse ratio at the mPP to DG synapses (Fig. 2 *C* and *D*) [genotype: $F(1, 56) = 0.0002$, $P = 0.99$] remained unchanged in slices from $SR^{-/-}$ mice. However, we observed significant deficits in LTP. Whereas the initial potentiation after the LTP-inducing high-frequency stimulation was similar between WT and $SR^{-/-}$ mice and likely reflects posttetanic potentiation or short-term potentiation, forms of synaptic plasticity independent of NMDAR activation (41), we found that the magnitude of LTP induced by a 1-s train of 100-Hz stimulations was significantly reduced in slices from $SR^{-/-}$ mice (Fig. 2 *E* and *F*) [genotype: $F(1, 120) = 7.53$, $P < 0.02$].

Reduced Spine Density in the Hippocampus of $SR^{-/-}$ Mice Is Associated with Altered miR-132 Expression. We next examined aspects of neuronal morphology in the $SR^{-/-}$ mouse hippocampus. Similar to observations in human schizophrenia, the $SR^{-/-}$ mice showed a small, but quite significant reduction in total hippocampal volume (Fig. 3*A*) ($P = 0.01$). Accompanying the reduction in hippocampal volume, we also observed a significant reduction in spine

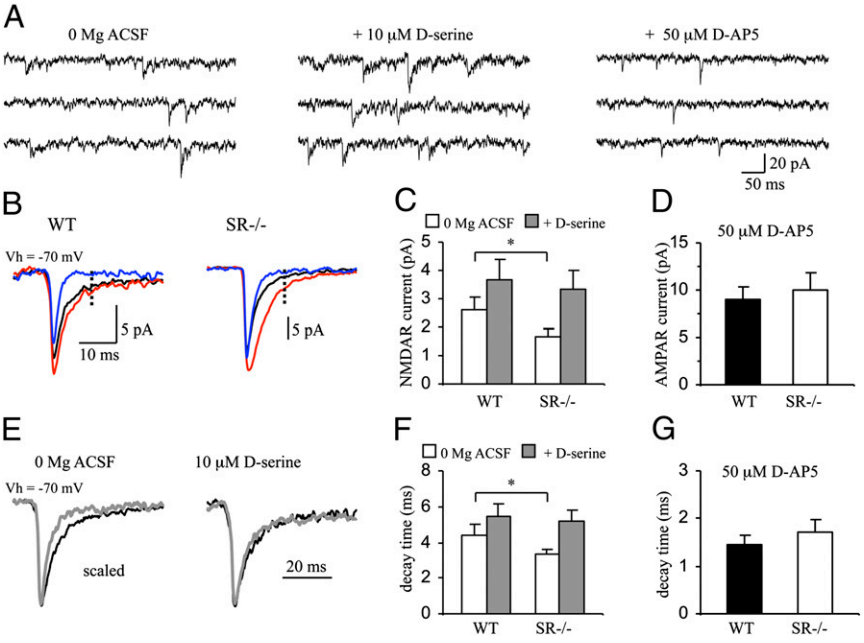

Fig. 1. NMDAR mEPSCs in DG granule cells are smaller and faster in $SR^{-/-}$ mice. (*A*) Examples of mEPSCs recorded from a DG granule cell at –70 mV in the absence of $Mg2^{+}$ (*Left*), in the presence of 10 μM D-serine (*Center*), and in the presence of 50 μM D-AP5 (*Right*). (*B*) Averaged mEPSCs (100–300 traces) recorded under control conditions (black), in the presence of D-serine (red), and in the presence of D-AP5 (blue) in slices from WT (*Left*) and $SR^{-/-}$ mice (*Right*). The amplitude of NMDAR mEPSCs were measured 10 ms after the peak (dashed line) of AMPAR currents in the presence of D-AP5. (*C*) Averaged amplitudes of NMDAR mEPSCs under different conditions. Data are from four WT ($n = 6$ cells) and four $SR^{-/-}$ ($n = 10$ cells) mice. (*D*) Averaged amplitudes of AMPAR mEPSCs in the presence of D-AP5 from three WT mice ($n = 5$ cells) and three $SR^{-/-}$ mice ($n = 7$ cells). (*E*) Superimposed averaged mEPSCs recorded from WT (black trace) and $SR^{-/-}$ mice (gray trace) under control conditions (*Left*) or in the presence of D-serine (*Right*). To ease the comparison of decay times, mEPSCs were scaled to the same peak amplitude. (*F*) Averaged decay times of mEPSCs. Data from four WT ($n = 6$ cells) and four $SR^{-/-}$ mice ($n = 10$ cells). (*G*) Averaged decay times of mEPSCs in the presence of D-AP5 from three WT ($n = 5$ cells) and three $SR^{-/-}$ ($n = 7$ cells) mice. Asterisk (*) indicates significant difference from the WT group ($P < 0.05$). All values represent the mean ± SEM.

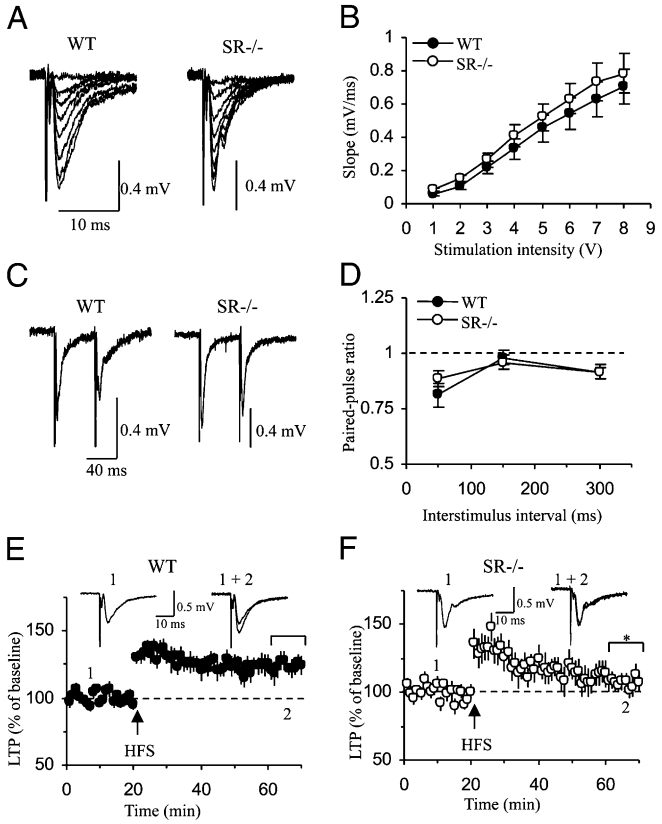

Fig. 2. LTP is suppressed at the mPP-DG synapses in $SR^{-/-}$ mice. (*A*) Averaged fEPSPs (10 traces) evoked at the mPP-DG synapses by presynaptic stimuli of increasing intensity in slices from WT (*Left*) and $SR^{-/-}$ mice (*Right*). (*B*) Synaptic input-output curves obtained in slices from six WT (n = 10 slices) and five $SR^{-/-}$ (n = 11 slices) mice. (*C*) Examples of fEPSPs at the mPP-DG synapses evoked with paired stimuli (interstimulus intervals 50-ms) in slices from WT (*Left*) and $SR^{-/-}$ mice (*Right*). (*D*) Averaged paired-pulse ratio values in slices from five WT (n = 11 slices) and five $SR^{-/-}$ (n = 18 slices) mice at interstimulus intervals 50, 150, and 300 ms. Paired-pulse ratio was calculated as the ratio of the rising slope of the second fEPSP to the first fEPSP. (*E* and *F*) Summary of LTP experiments from five WT mice (n = 8 slices) and four $SR^{-/-}$ mice (n = 8 slices). LTP was induced by a 1-s train of 100 Hz stimulation. *Insets* in *E* and *F* are the averages of: 1, 40 fEPSPs recorded before; 2, 20 fEPSPs recorded 40 min after the induction (at arrow) of LTP in slices from WT and $SR^{-/-}$ mice. Asterisk (*) indicates significant difference from the WT group ($P < 0.05$). All values represent the mean ± SEM.

density on dendritic arbors of DG granule neurons from $SR^{-/-}$ mice compared with WT mice (Fig. 3 *B* and *C*) ($P = 0.03$), similar to what we have observed in the cortex (42, 43). Consistent with these morphological abnormalities, the expression of miR-132, a known positive modulator of spine plasticity, was reduced. As shown in Fig. 3*D*, the expression of the primary ($P < 0.05$), precursor ($P < 0.05$), and mature ($P < 0.05$) transcripts of miR-132 were significantly reduced in $SR^{-/-}$ mice. We also examined mature miR-212 expression because it is processed from the same primary transcript as miR-132 (44). However, there was no difference in the expression of the mature miR-212 transcript in $SR^{-/-}$ mice (WT: 100 ± 0.1%; $SR^{-/-}$: 103 ± 0.09% $P = 0.86$). Others have also found changes in miR-132 expression without changes in miR-212 following manipulations in vivo (45).

BDNF Expression and TrkB Activation Are Reduced in the Hippocampus of $SR^{-/-}$ Mice. We next examined BDNF signaling in $SR^{-/-}$ mice because of its neurotrophic properties and link to NMDAR function. Using quantitative PCR (qPCR), we found that hippocampal BDNF mRNA was reduced in $SR^{-/-}$ mice (Fig. 4*A*) ($P < 0.05$). Cyclic AMP-responsive element binding protein (CREB) is a well-known transcriptional regulator of BDNF. The ability of CREB to regulate transcription is dependent, upon other things, its phosphorylation state at residue Serine 133 (pCREB Ser133). We found that nuclear pCREB Ser133 was reduced in the hippocampus of $SR^{-/-}$ mice (Fig. 4*B*) ($P < 0.05$), without a change in the total amount of nuclear CREB. Methyl CpG binding protein 2 (MeCP2) is a transcriptional repressor that negatively regulates BDNF expression (46). We found that although the mRNA ex-

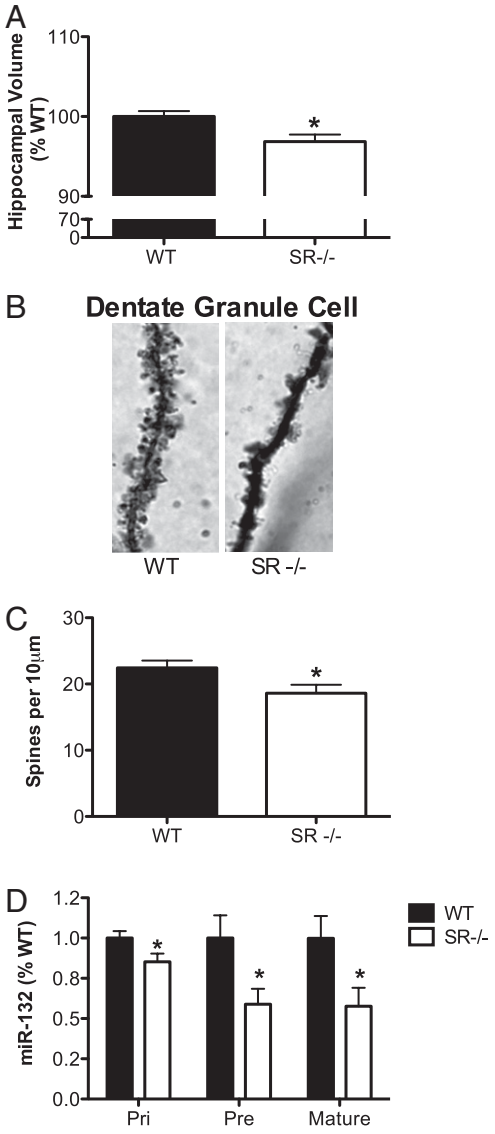

Fig. 3. Reduced dendritic spine density in the hippocampus of $SR^{-/-}$ mice is accompanied by altered miR-132 expression. (*A*) Hippocampal volume was estimated by the Cavaleri method on Nissl-stained coronal brain sections (n = 13–15/genotype). (*B*) Apical dendritic spines on a Golgi-stained granule (100x) cell in a WT (*Left*) and a $SR^{-/-}$ mouse (*Right*) (Magnification: 100×). (*C*) Spine density was compared between WT (n = 5) and $SR^{-/-}$ (n = 5) animals. Spine density on dentate granule neurons (three to six neurons per animal) was reduced on apical dendrites in $SR^{-/-}$ mice. Spine density is expressed as the number of spines per 10 μm of dendrite. (*D*) Relative expression of the primary (pri), precursor (pre), and mature miR-132 in WT (n = 7–11) and $SR^{-/-}$ (n = 7–11) mice were measured by qPCR. Data are expressed as geometric means ± SEM of individual expression values normalized to the appropriate reference gene (pri: GAPDH; pre: miR-16; mature miR-132/212: snoRNA-202) using the comparative $2^{-\Delta\Delta Ct}$ method. Asterisk (*) indicates significant difference from the WT group ($P < 0.05$). All values represent the mean ± SEM.

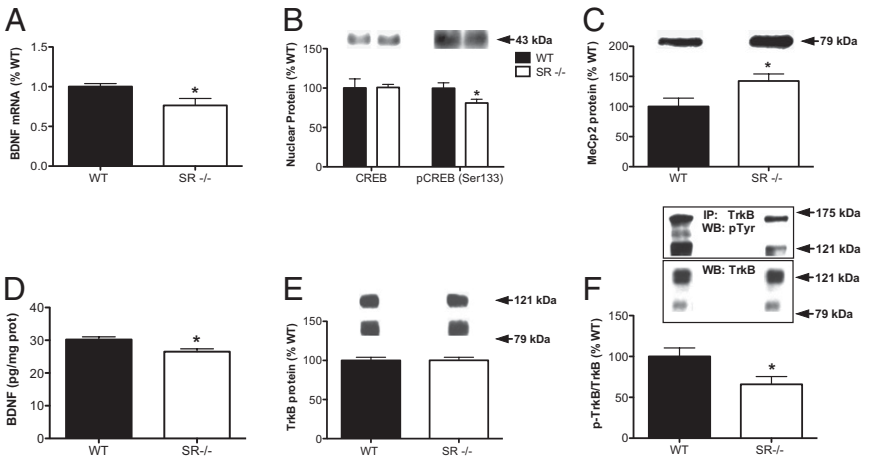

Fig. 4. BDNF expression and TrkB activation are reduced in the hippocampus of $SR^{-/-}$ mice. (*A*) Relative mRNA expression of BDNF obtained from the hippocampus of WT ($n = 6$; black bars) and $SR^{-/-}$ ($n = 5$; white bars) mice was measured by qPCR. Data are expressed as geometric means ± SEM of individual expression values normalized to the housekeeping gene GAPDH using the comparative $2^{-\Delta\Delta Ct}$ method. (*B*) Nuclear protein levels of CREB and p-CREB (Ser133) were measured by Western blot in the hippocampus of WT ($n = 5$–7) and $SR^{-/-}$ ($n = 6$–9) mice. (*C*) Nuclear protein levels of MeCP2 were measured by Western blot in the hippocampus of WT ($n = 12$) and $SR^{-/-}$ ($n = 10$) mice. (*D*) BNDF protein levels were measured in WT ($n = 7$) and $SR^{-/-}$ ($n = 6$) mice using ELISA. (*E*) TrkB protein levels were measured by Western blot from WT ($n = 13$) and $SR^{-/-}$ ($n = 14$) mice. (*F*) Hippocampal lysates from WT ($n = 10$) and $SR^{-/-}$ ($n = 10$) were subjected to immunoprecipitation with rabbit anti-TrkB antibody and immunoblotted with pY99 antibody. Immunoprecipitation of total TrkB was confirmed by immunoblotting with mouse-antiTrkB antibodies. Densitometric analyses are shown for p-TrkB receptor relative to the total TrkB obtained from immunoprecipitation. Asterisk (*) indicates significant differences from the WT group ($P < 0.05$). All values represent the mean ± SEM.

pression level of MeCP2 was unaltered in the hippocampus of $SR^{-/-}$ mice (WT: 100 ± 0.9%; $SR^{-/-}$: 103 ± 0.1%; $P = 0.85$), the amount of protein was significantly increased in the nucleus (Fig. 4*C*) ($P < 0.05$). Interestingly, MeCP2 mRNA is a known target for miR-132 degradation (47).

We next determined whether reduced BDNF mRNA was associated with reduced protein. We indeed found that $SR^{-/-}$ mice had significantly reduced levels of free, mature BDNF protein in the hippocampus (Fig. 4*D*) ($P = 0.01$). Although the total protein amount of TrkB was unchanged (Fig. 4*E*), the amount of phosphorylated (active) TrkB was reduced (Fig. 4*F*) ($P < 0.05$) in the hippocampus of $SR^{-/-}$ mice.

Akt/Mammalian Target of Rapamycin Signaling Is Reduced in the Hippocampus of $SR^{-/-}$ Mice. Given that $SR^{-/-}$ mice had reduced levels of BDNF and p-TrkB (activated), we examined the activity of signaling pathways downstream of TrkB. We found that although the total amount of Akt protein did not differ between genotypes, the amount of p-Akt (activated) was reduced in $SR^{-/-}$ mice (Fig. 5*A*) (Ser473: $P < 0.05$; Thr308: $P < 0.05$). In addition, the amount of p- mammalian target of rapamycin (p-mTOR) (Ser2448), which is phosphorylated by Akt, was reduced in $SR^{-/-}$ mice (Fig. 5*B*) ($P < 0.005$). The reduced levels of Akt (Ser473: $P < 0.01$; Thr308: $P < 0.05$) and mTOR phosphorylation ($P < 0.05$) were also found in the synaptoneurosomal fraction (Fig. 5 *F* and *G*). Because $SR^{-/-}$ mice have reduced spine density in the hippocampus, we examined downstream targets of mTOR signaling involved in protein synthesis. Although we did not find any changes in the protein levels or phosphorylation states of molecules downstream of mTOR in the whole-cell lysate (Fig. 5 *C–E*), we did find that $SR^{-/-}$ mice had significantly reduced phosphorylation of numerous proteins that regulate protein synthesis (Fig. 5 *H–J*) [p-p70S6 kinase: $P < 0.01$; p-4E-BP1 (eukaryotic translation initiation factor 4E-binding protein 1): $P < 0.05$; p-eEF2 (eukaryotic elongation factor 2): $P < 0.01$]. In contrast to Akt and mTOR signaling, MAPK and ERK (Table 1) signaling were not altered in the hippocampus of $SR^{-/-}$ mice.

Chronic Peripheral D-Serine Treatment Restores Brain D-Serine Levels in $SR^{-/-}$ Mice. We next wanted to determine whether the neuroplasticity deficits could be rescued in $SR^{-/-}$ mice following chronic D-serine treatment. We first measured D-serine content in the serum and in several brain regions to assess the effectiveness of our D-serine dosing regimen (Fig. 6 *A* and *B*). Vehicle-treated $SR^{-/-}$ mice had 30% less D-serine in the serum compared with vehicle-treated WT mice. Chronic D-serine treatment produced a fivefold elevation in serum D-serine levels in $SR^{-/-}$ mice (Fig. 6*C*) [$F(2, 9) = 29.5$, $P < 0.0001$]. $SR^{-/-}$ mice treated with D-serine also had sixfold higher cortical D-serine content than vehicle-treated $SR^{-/-}$ mice and 30% less D-serine than WT mice (Fig. 6*D*) [$F(2,10) = 90.6$, $P < 0.0001$]. However, in the hippocampus, D-serine–treated $SR^{-/-}$ mice had their D-serine levels completely restored to WT levels [$F(2, 6) = 13.3$, $P < 0.01$]. We also examined the kidneys of these mice because a single dose of D-serine (400 mg/kg) leads to transient nephrotoxicity in rats due to high levels of D-amino acid oxidase in the proximal tubules (48). We found that our chronic D-serine dosing regimen had no deleterious effects on the kidneys (Fig. 6 *E–G*), as evidenced by intact glomeruli.

Chronic D-Serine Treatment Reverses Neuroplasticity and Cognitive Deficits in $SR^{-/-}$ Mice. Chronic D-serine treatment completely rescued the LTP deficit at mPP-DG synapses in $SR^{-/-}$ mice (Fig. 7 *A–C)*) [$F(2, 20) = 43.8$, $P < 0.0001$]. LTP-induction in D-serine–treated $SR^{-/-}$ mice were also greater than that obtained in WT mice. Chronic injection stress did not affect the ability to induce LTP at the studied synapses [injected WT mice: noninjected WT mice; one-way repeated measures ANOVA, last 10 min of recording: $F(1, 170) = 0.7$, $P = 0.20$]. We next determined whether D-serine treatment could reverse the neurochemical abnormalities in $SR^{-/-}$ mice. Indeed, D-serine restored p-CREB [$F(2, 20) = 5.4$ $P < 0.02$] and MeCP2 [$F(2, 20) = 3.4$, $P < 0.05$] protein expression back to WT levels in $SR^{-/-}$ mice (Fig. 7*D*), which was paralleled by an increase in BDNF protein expression (Fig. 7*E*) [$F(2, 21) = 4.1$, $P < 0.05$]. This increase in BDNF was accompanied by a normalization of p-Akt (Fig. 7*F*) [Ser473: $F(2, 21) = 4.9$, $P < 0.02$; Thr308: $F(2, 21) = 5.0$, $P < 0.02$], and in particular p-Akt1 (Fig. 7*G*) [$F(2, 20) = 4.2$, $P < 0.05$], the isoform linked to schizophrenia. Activation of signaling molecules downstream of Akt, including p-mTOR (Fig. 7*H*) [Ser2448: $F(2, 21) = 4.3$, $P < 0.03$] and p-glycogen synthase kinase 3 (GSK3α) (Fig. 7*I*)

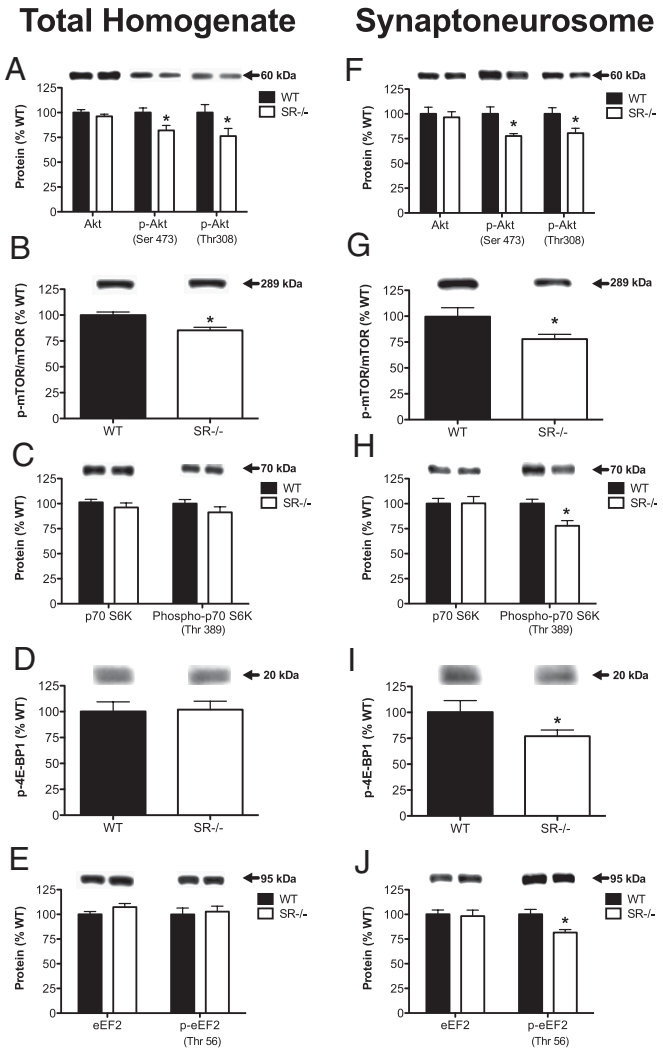

Fig. 5. Akt/mTOR signaling is reduced in the hippocampus of $SR^{-/-}$ mice. Protein levels of Akt/p-Akt (Ser473, Thr308), mTOR/p-mTOR (Ser2448), p70 S6 kinase/p-p70 S6K (Thr389), eEF2/p-eEF2 (Thr56), and 4-E-BP1/p-4E-BP1 (Thr37/46) were measured in the total homogenate (*A–E*) and synaptoneurosomal fractions (*F–J*) from the hippocampus of WT (n = 8–12; black bars) and $SR^{-/-}$ (n = 8–12; white bars) mice. Asterisk (*) indicates significant differences from the WT group ($P < 0.05$). All values represent the mean ± SEM.

[GSK3α: $F(2, 21) = 4.3$, $P < 0.05$; GSK3β: $F(2, 21) = 3.9$, $P < 0.05$] were also normalized in $SR^{-/-}$ mice following D-serine administration.

$SR^{-/-}$ mice have cognitive deficits likely caused by reduced D-serine levels in the brain. As such, we tested whether chronic D-serine administration could reverse the cognitive deficits observed in $SR^{-/-}$ mice. To this end, we chronically administered vehicle or D-serine to WT and $SR^{-/-}$ mice and tested them in a trace fear-conditioning paradigm (Fig. 7*J*) during the final 3 d of drug treatment to assess memory function. Unlike delay conditioning where the tone (conditioned stimulus, CS) and shock (unconditioned stimulus, US) coterminate (49), trace fear conditioning, which places a time interval between the CS and US, makes both the contextual and auditory memories hippocampal-dependent (50–53). Moreover, NMDARs in the hippocampus are also required for auditory (CS) memory following trace fear conditioning (51, 52). There was no difference in the amount of freezing at baseline or at the end of fear conditioning across groups on day 1 (Fig. S1 *A* and *B*). On day 2, $SR^{-/-}$ mice froze significantly less than WT mice when placed in the same context as day 1, a deficit that was completely reversed by D-serine (Fig. 7*K*) [$F(2,18) = 5.15$, $P < 0.03$]. When memory for the tone was assessed in a novel context on day 3, $SR^{-/-}$ mice exhibited reduced freezing compared with WT mice, which was again restored to WT levels by D-serine (Fig. 7*L*) [$F(2, 9) = 8.5$, $P < 0.01$]. D-serine also reversed the freezing deficit in $SR^{-/-}$ mice during the trace intervals on day 3 (Fig. S1*C*). The hot-plate assay revealed no difference in pain sensitivity between WT and $SR^{-/-}$ mice (Fig. S1 *D* and *E*).

Discussion

Our results demonstrate that the coagonist, D-serine, is crucial for proper NMDAR function and the maintenance of LTP in the adult DG. Morphological analysis of the $SR^{-/-}$ mouse hippocampus revealed reduced dendritic spine density and reduced hippocampal volume. These changes in the $SR^{-/-}$ mice were paralleled by decreased levels of miR-132 and BDNF, which are positive regulators of dendritic spine expression. Consistent with the reduction in BDNF protein levels, $SR^{-/-}$ mice had reduced TrkB phosphorylation, diminished Akt/mTOR signaling, and reduced activation of protein synthesis pathways, particularly in the synaptoneurosome fraction. Finally, the electrophysiological, biochemical, and cognitive deficits of $SR^{-/-}$ mice were ameliorated by chronic, peripheral administration of D-serine.

NMDAR mEPSCs in DG granule cells were significantly smaller and exhibited faster decay times in $SR^{-/-}$ mice. Exogenously applied D-serine increased NMDAR mEPSCs in $SR^{-/-}$ mice twofold, indicating that under basal conditions of synaptic transmission the endogenous concentration of D-serine is decreased in the DG of $SR^{-/-}$ mice. D-serine has recently been shown to be responsible for regulating synaptic NMDARs in CA1 of the hippocampus through GluN2A-containing NMDARs (54). The partial deficit in NMDAR mEPSCs observed here in the DG and previously in the amygdala (55) from $SR^{-/-}$ mice suggests that the relative contribution of D-serine might vary depending on the synapse. This finding could be because of a number of factors, including differential NMDAR subunit composition, as the DG has a greater expression of GluN2B compared with CA1 (56). Consistent with the role of NMDARs in mPP-DG LTP (57), we found that LTP in the mPP-DG was diminished in slices from $SR^{-/-}$ mice. These observations provide further evidence for the role of endogenous D-serine in the

Table 1. MEK and ERK signaling is unaltered in the hippocampus of $SR^{-/-}$ mice

	MEK		p-MEK		ERK-42		p-ERK-42		ERK-44		p-ERK-44	
WT or SR	% WT	P	% WT	P	% WT	P	% WT	P	% WT	P	% WT	P
WT	100 ± 5	0.9	100 ± 12	0.4	100 ± 4	0.5	100 ± 8	0.7	100 ± 8	0.5	100 ± 15	0.8
$SR^{-/-}$	101 ± 6		88 ± 9		97 ± 4		95 ± 6		94 ± 7		92 ± 19	

Protein levels of MAP kinase kinase (MEK-1/2), p-MEK (Ser218/Ser222), p44/42 MAPK (ERK-1/2), and phospho-ERK-1/2 (pERK; Thr202/Tyr204) were measured in the total hippocampal homogenate from WT (n = 6) and $SR^{-/-}$ (n = 6) mice. Values are expressed as the optical density (OD) normalized to WT values (% WT). All values represent the mean ± SEM.

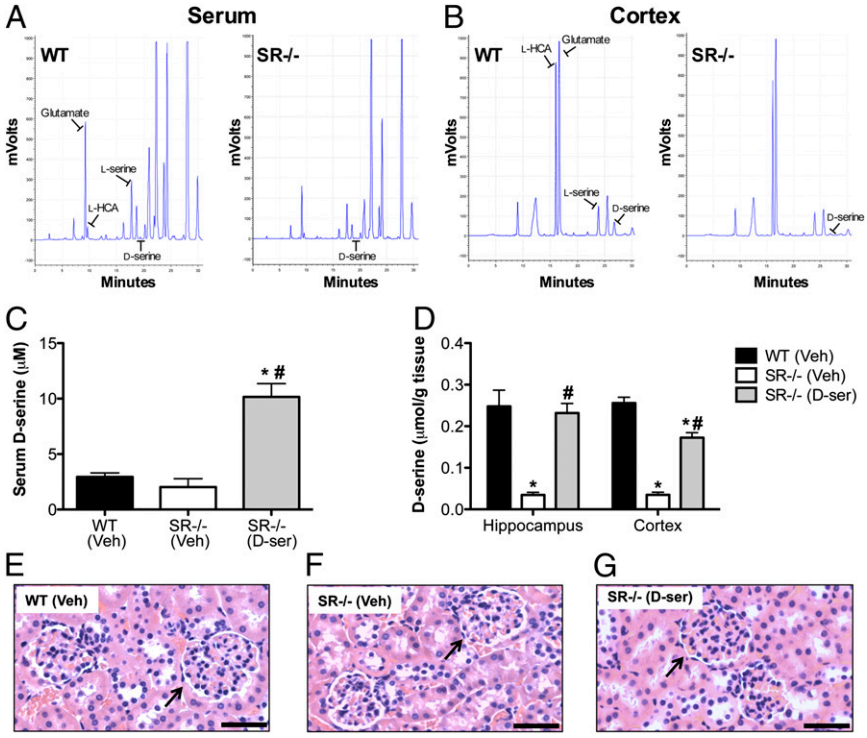

Fig. 6. Chronic peripheral administration of D-serine elevates serum and normalizes brain D-serine levels in $SR^{-/-}$ mice. WT and $SR^{-/-}$ mice received 21 d of either vehicle or D-serine (300 mg/kg day 1, 150 mg/kg days 2–21; s.c.) and were killed 24 h after the last injection. HPLC (HPLC) was used to quantify D-serine levels with representative chromatographs for WT and $SR^{-/-}$ serum and cortex samples shown. (*A*) (*Left*) Amino acid peaks and retention times of a WT serum sample. Glutamate (9 min), L-HCA (9.5 min), L-serine (18 min), and D-serine (19 min) are indicated. (*Right*) A slight reduction in D-serine in a $SR^{-/-}$ serum sample compared with WT. (*B*) (*Left*) Amino acid peaks and retention times of a WT cortical sample. Glutamate (16.5 min), L-HCA (16 min), L-serine (24 min), and D-serine (27 min) are indicated. (*Right*) A marked reduction in D-serine in a $SR^{-/-}$ cortical sample compared with WT. (*C* and *D*) D-serine was measured in the serum, hippocampus, and cortex of WT (vehicle; n = 4–5; black bars), $SR^{-/-}$ mice (vehicle; n = 3–4; white bars), and $SR^{-/-}$ mice treated with D-serine (n = 2–4; gray bars). Significant one-way ANOVA results were followed up by Newman–Keuls Multiple comparison test. Asterisk (*) indicates significant difference from the WT group ($P < 0.05$) and a pound sign (#) indicates significant difference from the $SR^{-/-}$ vehicle group. All values represent the mean ± SEM. (*E–G*) H&E-stained kidneys (40×) from WT (*E*; vehicle), $SR^{-/-}$ (*F*; vehicle), and $SR^{-/-}$ mice treated with D-serine (*G*). Glomeruli (arrows) from D-serine treated mice do not show signs of necrosis. (Scale bars, 50 μm.)

mechanisms of long-term synaptic plasticity in hippocampal circuits (36, 54). The observed modulatory actions of D-serine on LTP were not because of an overall impairment in glutamatergic neurotransmission, as the functional properties of AMPARs were unaffected in $SR^{-/-}$ mice. Future studies will need to examine the molecular mechanisms underlying the LTP deficits.

Dendritic spine plasticity is regulated by many factors. We found that two known regulators of dendritic spines, miR-132 and BDNF, were perturbed in the hippocampus of $SR^{-/-}$ mice. BDNF and miR-132, the expression of which are regulated by NMDAR activity, were reduced in the hippocampus of $SR^{-/-}$ mice. The directionality of these changes is consistent with their roles as positive modulators of spine density and neuroplasticity, as well as with the schizophrenia postmortem findings. The expression of BDNF mRNA and protein is reduced in the dorsolateral prefrontal cortex (PFC) of subjects with schizophrenia (8); another study demonstrated a positive correlation between reduced BDNF mRNA levels and reduced spine density in the same subjects with schizophrenia (58). miR-132 expression is reduced in the PFC from subjects with schizophrenia and in the PFC of adult mice chronically treated during postnatal development with the noncompetitive NMDAR antagonist MK-801 (18). Further experiments will be needed to directly test whether the spine deficits in $SR^{-/-}$ mice are caused by abnormalities in BDNF or miR-132 expression.

The regulation of gene expression is a complex process that is achieved through balancing transcriptional activation and repression. NMDAR activity regulates BDNF and miR-132 expression, in part through affecting signaling cascades that ultimately modulate CREB-dependent and MeCP2-dependent transcriptional activation and suppression, respectively (22). The reduced expression of BDNF levels and the primary, precurser, and mature miR-132 transcripts in $SR^{-/-}$ mice were accompanied by reduced nuclear p-CREB-Ser133. Calcium influx following NMDAR activation triggers CREB phosphorylation at Ser residues, thereby facilitating transcription (22). In particular, pCREB-Ser133 is important for inducing BDNF transcription following physiological stimulation (59). Although miR-132 was initially identified in a genome-wide screen for CREB-binding sites that are tightly associated with miRs (60), it is unknown if phosphorylation at Ser133 is important for its transcriptional activation. In opposition to CREB, MeCP2 represses gene transcription by binding to methylated DNA and recruiting enzymes that modify histones (22). MeCP2 is a well-known repressor of BDNF expression (22) and has also recently been shown to reduce the expression of miR-132 in vitro and in vivo (61). Because the MeCP2 mRNA transcript is a target for miR-132, the reduced miR-132 levels in $SR^{-/-}$ mice could be contributing to the elevated MeCP2 protein via translational inhibition, as we found no change in MeCP2 mRNA expression. Therefore, the reduced miR-132 expression in $SR^{-/-}$ mice could also be indirectly reducing BDNF expression by, in part, increasing the amount of MeCP2. Given the complex feedback nature of this signaling network, future experiments will be needed to elucidate which are the upstream regulatory elements.

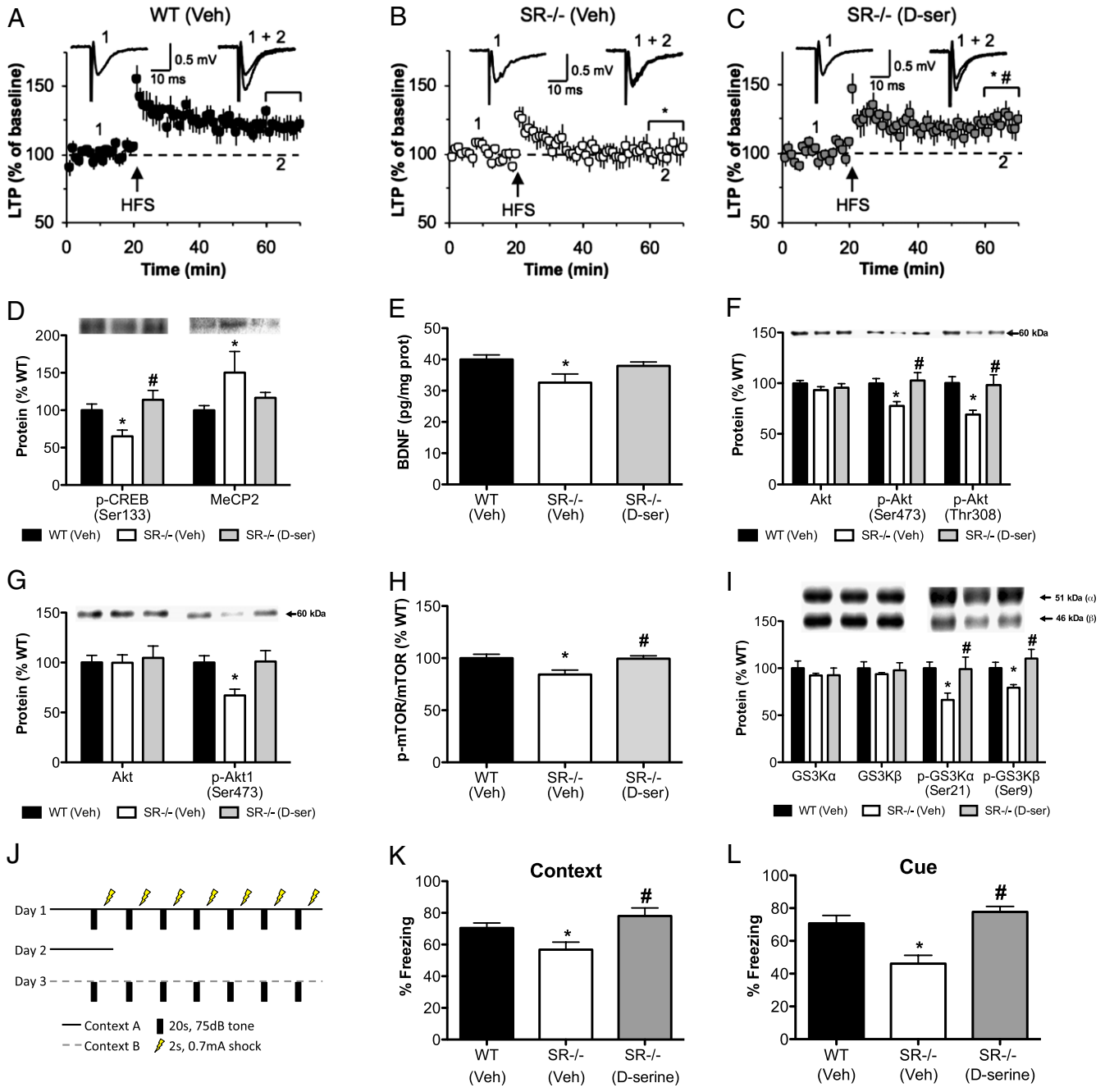

Fig. 7. Chronic D-serine treatment reverses the electrophysiological, biochemical, and cognitive deficits found in $SR^{-/-}$ mice. WT and $SR^{-/-}$ mice received 21 d of either vehicle or D-serine (300 mg/kg day 1, 150 mg/kg days 2–21; s.c.) and were killed 24 h after the last injection. (*A–C*) Summary of LTP experiments at the mPP-DG synapses from five WT (n = 10 slices; black circles) mice receiving vehicle injections, four $SR^{-/-}$ mice (n = 9 slices; white circles) receiving vehicle injections, and four $SR^{-/-}$ (n = 8 slices; gray circles) mice receiving chronic D-serine injections. *Insets* are the averages of: 1, 40 fEPSPs recorded before; and 2, 20 fEPSPs recorded 40 min after the induction of LTP (at arrow). Significant one-way repeated measures ANOVA during the last 10 min of recording was followed up by Bonferroni's multiple comparison test. Protein levels of (*D*) p-CREB and MeCP2, (*E*) BDNF, (*F*) Akt/p-Akt (Ser473, Thr308), (*G*) Akt1/p-Akt1 (Ser473), (*H*) mTOR/p-mTOR (Ser2448), and (*I*) GSK3α Ser21/β Ser9 were measured in the hippocampus of WT (n = 12; black bars), $SR^{-/-}$ (n = 5–6; white bars), and $SR^{-/-}$ mice treated with D-serine (n = 5–6; gray bars). BDNF values are expressed as pg of BDNF/mg of protein. Significant one-way ANOVA results were followed up by Newman–Keuls Multiple comparison test. (*J*) Diagram illustrating the trace fear-conditioning paradigm. WT (n = 11), $SR^{-/-}$ (n = 5), and $SR^{-/-}$ mice treated with D-serine (n = 5) were subjected to the paradigm during the last 3 d of treatment. Injections were given 3 h before behavioral testing. (*K*) Representation of the average time animals froze during the first 3 min of being placed in the chamber on day 2. (*L*) Represents the average freezing of each mouse during the seven, 20-s tone presentations on day 3. Asterisk (*) indicates significant difference from the WT group ($P < 0.05$) and pound symbol (#) indicates significant difference from the $SR^{-/-}$ vehicle group. All values represent the mean ± SEM.

Local protein synthesis is necessary for dendritic plasticity (62), as activation of the Akt/mTOR/p70S6K pathway increases dendritic arborization and spine density (63, 64). Thus, attenuated mTOR signaling in $SR^{-/-}$ mice could be in part, responsible for the reduced dendritic spine density in the DG. NMDAR activity also modulates the elongation step of protein synthesis

through regulation of eEF2, a GTP-binding protein that controls mRNA trafficking through the ribosome. Although phosphorylation of eEF2 on Thr56 usually inhibits eEF2-ribosome binding and arrests peptide chain elongation (65), it also increases the translation of some mRNAs localized to dendrites (66, 67). Reducing the amount of p-eEF2 decreases hippocampal spine density and stability, as well as dendritic BDNF protein expression (68). Hence, impaired eEF2 signaling in the hippocampal synaptoneurosome fraction of $SR^{-/-}$ mice could be another contributing factor to not only the reduced spine density, but also the reduced BDNF protein levels.

The mTORC1 pathway described above can be activated by NMDAR activity and by neurotrophins, such as BDNF. NMDAR and TrkB activation lead to increases in both PI3K/Akt and MAPK/ERK signaling. Activation of these two pathways relieves the constitutive inhibition placed on the mTORC1 complex and increases protein synthesis. Akt signaling, but not MAPK/ERK signaling, was reduced in the hippocampus of $SR^{-/-}$ mice. This finding suggests that attenuated Akt activity is contributing to the reduced levels of p-mTOR and subsequent impaired mTORC1 signaling. Interestingly, *AKT1* has been associated with an increased risk for schizophrenia (13). Furthermore, reduced Akt signaling likely contributes to the pathophysiology of the disorder, as the brains of patients with schizophrenia have reduced Akt and p-Akt levels (16, 69). Evidence from genetic animal models also implicates Akt1 in processes that are altered in patients with schizophrenia, including hippocampal plasticity (i.e., LTP) and cognitive tasks (16, 70). We demonstrate here that $SR^{-/-}$ mice have reduced hippocampal p-Akt1, which fully accounts for the reduction in total p-Akt (Fig. 7) and highlights the importance of this particular isoform of Akt in the brain. Thus, impaired Akt1 signaling in the hippocampus of $SR^{-/-}$ mice potentially contributes to the reductions in spine density and neuroplasticity via mTORC1.

Although the current medications for schizophrenia, which mainly block dopamine D2 receptors, are relatively effective in managing the psychosis, they are ineffective in treating the cognitive deficits and negative symptoms (71). These deficits are the most enduring and correlate with the degree of cortical atrophy. A recent meta-analysis found that GMS agonists, including D-serine, exert significant therapeutic effects on multiple symptom domains in schizophrenia in patients receiving antipsychotic medications, especially negative and cognitive symptoms (72). We found that chronic, peripherally administered D-serine to $SR^{-/-}$ mice normalized the LTP deficit at the mPP-DG synapse, MeCP2, pCREB, and BDNF protein expression, as well as downstream Akt/mTOR/GS3K signaling. Our previous research has demonstrated that $SR^{-/-}$ mice have impairments in spatial and contextual memory (36, 73). We demonstrate here that $SR^{-/-}$ mice also have impairments in fear-conditioned learning that can be rescued by D-serine treatment. Specifically, $SR^{-/-}$ mice have impairments in contextual and cue-dependent memory following trace fear conditioning. The introduction of the trace interval during conditioning makes both the contextual and auditory memories hippocampal-dependent, as determined by lesion (50, 53) and NMDAR antagonist infusion (51, 52) studies. Thus, normalizing NMDAR activity in $SR^{-/-}$ mice with D-serine treatment was able to rescue deficits in both contextual and auditory trace fear conditioning. Future studies will need to determine the duration of treatment needed for the restorative effects of D-serine, as well as which signaling pathways downstream of NMDAR activation and which brain regions are critical for the cognitive enhancing effects.

In conclusion, $SR^{-/-}$ mice display significant impairments in hippocampal neuroplasticity, both at the electrophysiological and neurochemical level. Importantly, NMDAR hypofunction alters numerous pathways, including BDNF/TrkB, Akt/mTOR/GS3K, and miR-132 that not are not only potent regulators of plasticity and spine dynamics, but have been found to be genetically associated with or perturbed in schizophrenia (13). Furthermore, a recent study of de novo copy number variants implicated in schizophrenia demonstrated a highly significant enrichment of gene products that are localized to the postsynaptic density and are associated with the NMDAR (28). Thus, morphological, neurochemical, functional and cognitive deficits of the hippocampus and cortex demonstrated in schizophrenia can be recapitulated in the mouse by reduced availability of D-serine, one of the two coagonists at the NMDAR, resulting in NMDAR hypofunction (Table S1). Finally, these findings demonstrate that neuroplasticity and behavioral deficits resulting from a constitutive genetic lesion can be reversed with interventions that occur in adulthood and highlight the GMS on the NMDAR as a potential therapeutic target for schizophrenia.

Materials and Methods

Further details on subcellular fractionation, Western blot analysis, HPLC, kidney staining, trace fear conditioning, and hot-plate test can be found in the *SI Materials and Methods*.

Animals. $SR^{-/-}$ mice (36) were generated as previously described. $SR^{+/-}$ sires and dams were bred to produce WT and $SR^{-/-}$ offspring. Adult male mice (3–5 mo old) were used for all of the experiments, except where noted. Animals were housed in groups of four in polycarbonate cages and maintained on a 12:12-h light/dark cycle in a temperature (22 °C) and humidity controlled vivarium. Animals were given access to food and water ad libitum. All animal procedures were approved by the McLean Hospital Institutional Animal Care and Use Committee.

Electrophysiology. Hippocampal slices (400 μm) were prepared from adult $SR^{-/-}$ or WT mice (littermates) with a vibratome. Slices were continuously perfused in solution containing: 119 mM NaCl, 2.5 mM KCl, 2.5 mM $CaCl_2$, 1.0 mM $MgSO_4$, 1.25 mM NaH_2PO_4, 26.0 mM $NaHCO_3$, 10 mM glucose, and 0.05 mM picrotoxin, and equilibrated with 95% (vol/vol) O_2 and 5% CO_2 (pH 7.3–7.4) at 22 °C. fEPSPs were recorded in the middle molecular layer of the DG of the hippocampus with a glass pipette filled with the extracellular solution. Synaptic responses were evoked at 0.033 Hz by stimulation of the mPP (74, 75) with a concentric stimulation electrode (76, 77). In LTP experiments, the baseline stimulation intensity was adjusted to produce fEPSPs with an amplitude that was ~30% of maximum amplitude fEPSP. LTP was induced by a 1-s train of presynaptic stimulation at 100 Hz. The initial slope of the fEPSP's rising phase was used to measure the changes in synaptic strength. Summary LTP graphs were constructed by normalizing data in 60-s epochs to the mean value of the baseline fEPSPs slope. The magnitude of LTP was estimated in a 10-min time window 40 min after the induction. Whole-cell recordings (2- to 7-mo-old male and female mice; groups were counterbalanced for age and sex) of spontaneous mEPSCs were obtained from granule cells of the DG at physiological temperature (36 ± 1°) in the presence of 1 μM tetrodotoxin (TTX) to block action potential-induced neurotransmitter release. The NMDAR-mediated currents were recorded under voltage-clamp conditions at –70 mV without Mg^{2+} in the external medium. The patch electrodes (3–4 MΩ resistance) in voltage-clamp experiments contained: 120 mM Cs-methanesulfonate, 5 mM NaCl, 1 mM $MgCl_2$, 10 mM BAPTA, 10 mM Hepes, 2 mM Mg-ATP, and 0.1 mM Na-GTP (adjusted to pH 7.2 with CsOH). Spontaneous synaptic currents were filtered at 1 kHz and digitized at 5 kHz. The mEPSCs were recorded first in control external solution, then in the presence of 10 μM D-serine, and, finally, in the presence of the NMDA receptor antagonist D-AP5 (50 μM). Series resistance was monitored throughout the experiment and was in the range of 15–25 MΩ. The parameters of mEPSCs were analyzed with the Mini Analysis Program (Synaptosoft).

Golgi Staining and Quantification of Dendritic Spine Density. Golgi staining was performed using the FD Rapid GolgiStain Kit (FD NeuroTechnologies) as previously described (42, 43, 78). Neurons were located between approximately –1.46 mm to –2.20 mm posterior to bregma (79) and within the middle third of the section. Spines were counted on two unobscured apical dendritic branches (minimum second order) per neuron, with the average spine density used as the value for that neuron. Spines were counted on three to six neurons per animal. Only neurons in the outer two-thirds of the granule cell layer of the DG were chosen for spine density analysis. Neurons in the outer layers of the granule cell layer are not derived from the actively dividing cells of the subgranular zone associated with adult neurogenesis. The average dendritic length analyzed for spine density did not significantly differ between genotypes (WT = 28.9 ± 0.8 μm, $SR^{-/-}$ = 32.0 ± 1.9 μm).

Dendrites were visualized at 100× (oil-immersion) on a Zeiss Axioskop40 microscope and the number of spines was quantified using Neurolucida (MBF Bioscience). The experimenter was blind to genotype during tracing.

Nissl Staining and Hippocampal Volume Estimation. Brains from WT and $SR^{-/-}$ were fixed, sectioned, and stained using cresyl echt violet solution (pH 3.5) as previously described (78). Hippocampal volume was estimated at 4× on a Zeiss Axioskop40 by the Cavalieri method (600-μm grid size; 7–9 sections per brain) using Stereo Investigator software (MBF Bioscience). The grid size chosen estimated volumes with high precision (coefficient of error: 0.009; average total points per hippocampus: 177).

qPCR. RNA was isolated from the hippocampi of WT and $SR^{-/-}$ mice (n = 6/genotype) as previously described (78). RNA was isolated from the tissue samples using the miRvana miRNA isolation kit (Ambion). cDNA for each RNA sample (2-μg input) was generated using the High Capacity cDNA Reverse Transcription kit (Applied Biosystems). Mature miR-132 and sno-202 cDNA (10-ng input) was generated using the TaqMan MicroRNA Reverse Transcription kit (Applied Biosystems). premiR-132 (10-μm primer) and miR-16 (10-μm primer) cDNA (500-ng input) were generated using the SuperScript III First-Strand Synthesis System (Invitrogen). An initial step of 80 °C for 1 min was added to the SuperScript III protocol to denature the hairpin structures in premiR-132 transcripts. The primers and protocol were based on a previous study (80). qPCR for GAPDH, BDNF, and pri-miR-132 were performed using TaqMan gene expression assays (Applied Biosystems). Data were collected using a 48-well MJ Minioption Personal thermal cycler (Bio-Rad). qPCR for mature miR-132 and snoRNA202 was performed using the TaqMan MicroRNA expression assays (Applied Biosystems). qPCR for premiR-132 and miR-16 was performed using the Platinum SYBR Green qPCR SuperMix UDG (Invitrogen), which was followed by a thermal denaturation protocol to ensure amplification of a single product. For relative quantification of mRNA expression (BDNF, MeCP2, pri-miR132), geometric means were calculated using the comparative $2^{-\Delta\Delta Ct}$ method, with the housekeeping gene GAPDH used as the endogenous reference. miR-16 and snoRNA202 were used as the endogenous reference genes for premiR-132 and mature miR-132, respectively. Each sample was assayed in triplicate. All primers are listed in Table S2.

BDNF ELISA. BDNF levels from the hippocampi of WT and $SR^{-/-}$ mice were measured using a commercially available ELISA kit (Promega) as previously described (78)

Subcellular Fractionation. The fractionation procedure was modified from a previously published protocol (81). Protein concentrations were measured using the Bradford protein assay (Bio-Rad).

Western Blot Analysis. Immunoblotting was performed as previously described (81). Primary antibodies are listed in Table S3. Chemiluminescent values of the protein of interest were divided by its corresponding β-actin chemiluminescent values. The ratio of each WT sample was divided by the average of all of the WT sample values in each gel and multiplied by 100. The average of the normalized WT values from each gel was 100% ± SEM. The mutant values were normalized to WT values (percent of WT) collected in parallel from the same gel. The normalized values were then averaged and used for statistical analysis.

Immunoprecipitation. A separate cohort of mice from the ELISA and Western blot analyses was used for immunoprecipitation. Hippocampal tissue lysate was immunoprecipitated with a TrkB antibody. TrkB phosphorylation was measured by immunoblotting for phosphotyrosine, stripping the membrane, and then reprobing for TrkB.

Chronic D-Serine Treatment. Mice received once daily, subcutaneous injections of vehicle or D-serine for 20 d at a volume of 5 mL/kg. WT mice received vehicle (0.9% sodium chloride) and $SR^{-/-}$ mice received either vehicle or D-serine (Sigma-Aldrich). D-serine was given at an initial dose of 300 mg/kg on day 1, followed by 150 mg/kg for the remaining 20 d. Mice were killed on day 21 without receiving an injection. One hippocampal lobe was used for electrophysiology and the other lobe was used for neurochemistry. Left and right hemispheres were counterbalanced for analysis.

HPLC Analysis of D-Serine. Brain tissue and trunk blood were obtained from the same chronically treated mice that were used in the LTP experiments. Blood was collected, allowed to clot for 10 min, and spun at 2,000 × g for 15 min at room temperature. Brain tissue and serum content of D-serine were analyzed as previously described (36, 82).

Trace Fear Conditioning. Mice were subjected to a trace fear conditioning protocol adapted from ref. 50. Mice were trained in context A on day 1. Memory for context A was measured on day 2 and memory for the CS (tone) in context B was measured on day 3. All testing was performed using the The Near Infrared Fear Conditioning System (Med Associates). Freezing behavior was quantified using VideoFreeze software.

Statistical Analyses. Dendritic spine density, Western blot, qPCR, and BDNF ELISA results were compared using unpaired Student t test. Repeated measures one-way ANOVA was used to analyze LTP results, and one-way ANOVA was used to analyze BDNF, Western blot, and fear conditioning results following chronic D-serine treatment. Significant F values were subject to post hoc analyses as indicated. Values of $P < 0.05$ were considered statistically significant.

ACKNOWLEDGMENTS. We thank Drs. Sabina Berretta, Ole Isacson, and Uwe Rudolph for the generous use of their equipment and software; Dr. Christopher Cowan for advice; and Jiamin Feng for animal colony maintenance and genotyping. The Rodent Histopathology Core Facility of the Dana-Farber/Harvard Cancer Center (P30 CA06516) performed the kidney staining. Phenopro performed the hot-plate test. This work was supported in part by a postdoctoral National Research Service Award F32 MH090697; an Andrew P. Merrill Research Fellowship; a Phyllis & Jerome Lyle Rappaport Mental Health Research Scholars Award (to D.T.B.); and National Institutes of Health Grants R01MH05190 and P50MH0G0450 (to J.T.C.).

1. Perälä J, et al. (2007) Lifetime prevalence of psychotic and bipolar I disorders in a general population. *Arch Gen Psychiatry* 64(1):19–28.
2. Jarskog LF, Miyamoto S, Lieberman JA (2007) Schizophrenia: New pathological insights and therapies. *Annu Rev Med* 58:49–61.
3. Rosoklija G, et al. (2000) Structural abnormalities of subicular dendrites in subjects with schizophrenia and mood disorders: Preliminary findings. *Arch Gen Psychiatry* 57(4):349–356.
4. Adriano F, Caltagirone C, Spalletta G (2011) Hippocampal volume reduction in first-episode and chronic schizophrenia: A review and meta-analysis. *Neuroscientist* 18(2): 180–200.
5. Heckers S, et al. (1998) Impaired recruitment of the hippocampus during conscious recollection in schizophrenia. *Nat Neurosci* 1(4):318–323.
6. Binder DK, Scharfman HE (2004) Brain-derived neurotrophic factor. *Growth Factors* 22(3):123–131.
7. Hashimoto T, et al. (2005) Relationship of brain-derived neurotrophic factor and its receptor TrkB to altered inhibitory prefrontal circuitry in schizophrenia. *J Neurosci* 25(2):372–383.
8. Weickert CS, et al. (2003) Reduced brain-derived neurotrophic factor in prefrontal cortex of patients with schizophrenia. *Mol Psychiatry* 8(6):592–610.
9. Wong J, et al. (2010) Promoter specific alterations of brain-derived neurotrophic factor mRNA in schizophrenia. *Neuroscience* 169(3):1071–1084.
10. Weickert CS, et al. (2005) Reductions in neurotrophin receptor mRNAs in the prefrontal cortex of patients with schizophrenia. *Mol Psychiatry* 10(7):637–650.
11. Thompson Ray M, Weickert CS, Wyatt E, Webster MJ (2011) Decreased BDNF, trkB-TK+ and GAD67 mRNA expression in the hippocampus of individuals with schizophrenia and mood disorders. *J Psychiatry Neurosci* 36(3):195–203.
12. Wong J, Rothmond DA, Webster MJ, Shannon Weickert C (2011) Increases in two truncated TrkB isoforms in the prefrontal cortex of people with schizophrenia. *Schizophr Bull* 39(1):130–140.
13. Balu DT, Coyle JT (2011) Neuroplasticity signaling pathways linked to the pathophysiology of schizophrenia. *Neurosci Biobehav Rev* 35(3):848–870.
14. Emamian ES, Hall D, Birnbaum MJ, Karayiorgou M, Gogos JA (2004) Convergent evidence for impaired AKT1-GSK3beta signaling in schizophrenia. *Nat Genet* 36(2): 131–137.
15. Thiselton DL, et al. (2008) AKT1 is associated with schizophrenia across multiple symptom dimensions in the Irish study of high density schizophrenia families. *Biol Psychiatry* 63(5):449–457.
16. Balu DT, et al. (2012) Akt1 deficiency in schizophrenia and impairment of hippocampal plasticity and function. *Hippocampus* 22(2):230–240.
17. Miller BH, Wahlestedt C (2010) MicroRNA dysregulation in psychiatric disease. *Brain Res* 1338:89–99.
18. Miller BH, et al. (2012) MicroRNA-132 dysregulation in schizophrenia has implications for both neurodevelopment and adult brain function. *Proc Natl Acad Sci USA* 109(8): 3125–3130.
19. Wayman GA, et al. (2008) An activity-regulated microRNA controls dendritic plasticity by down-regulating p250GAP. *Proc Natl Acad Sci USA* 105(26):9093–9098.
20. Nudelman AS, et al. (2009) Neuronal activity rapidly induces transcription of the CREB-regulated microRNA-132, in vivo. *Hippocampus* 20(4):492–498.

21. Tognini P, Putignano E, Coatti A, Pizzorusso T (2011) Experience-dependent expression of miR-132 regulates ocular dominance plasticity. *Nat Neurosci* 14(10):1237–1239.
22. Greer PL, Greenberg ME (2008) From synapse to nucleus: Calcium-dependent gene transcription in the control of synapse development and function. *Neuron* 59(6): 846–860.
23. Coyle JT (2006) Glutamate and schizophrenia: Beyond the dopamine hypothesis. *Cell Mol Neurobiol* 26(4-6):365–384.
24. Krystal JH, et al. (1994) Subanesthetic effects of the noncompetitive NMDA antagonist, ketamine, in humans. Psychotomimetic, perceptual, cognitive, and neuroendocrine responses. *Arch Gen Psychiatry* 51(3):199–214.
25. Weickert CS, et al. (2012) Molecular evidence of N-methyl-D-aspartate receptor hypofunction in schizophrenia. *Mol Psychiatry*, 10.1038/mp.2012.137.
26. Steiner J, et al. (2013) Increased prevalence of diverse N-methyl-D-aspartate glutamate receptor antibodies in patients with an initial diagnosis of schizophrenia: Specific relevance of IgG NR1a antibodies for distinction from N-methyl-D-aspartate glutamate receptor encephalitis. *JAMA Psychiatry* 70(3):271–278.
27. Allen NC, et al. (2008) Systematic meta-analyses and field synopsis of genetic association studies in schizophrenia: The SzGene database. *Nat Genet* 40(7):827–834.
28. Kirov G, et al. (2012) De novo CNV analysis implicates specific abnormalities of postsynaptic signalling complexes in the pathogenesis of schizophrenia. *Mol Psychiatry* 17(2):142–153.
29. Walsh T, et al. (2008) Rare structural variants disrupt multiple genes in neurodevelopmental pathways in schizophrenia. *Science* 320(5875):539–543.
30. Schell MJ, Molliver ME, Snyder SH (1995) D-serine, an endogenous synaptic modulator: Localization to astrocytes and glutamate-stimulated release. *Proc Natl Acad Sci USA* 92(9):3948–3952.
31. Bendikov I, et al. (2007) A CSF and postmortem brain study of D-serine metabolic parameters in schizophrenia. *Schizophr Res* 90(1–3):41–51.
32. Goltsov AY, et al. (2006) Polymorphism in the 5′-promoter region of serine racemase gene in schizophrenia. *Mol Psychiatry* 11(4):325–326.
33. Labrie V, Wang W, Barger SW, Baker GB, Roder JC (2009) Genetic loss of D-amino acid oxidase activity reverses schizophrenia-like phenotypes in mice. *Genes Brain Behav* 9(1):11–25.
34. Morita Y, et al. (2007) A genetic variant of the serine racemase gene is associated with schizophrenia. *Biol Psychiatry* 61(10):1200–1203.
35. Hashimoto K, et al. (2005) Reduced D-serine to total serine ratio in the cerebrospinal fluid of drug naive schizophrenic patients. *Prog Neuropsychopharmacol Biol Psychiatry* 29(5):767–769.
36. Basu AC, et al. (2009) Targeted disruption of serine racemase affects glutamatergic neurotransmission and behavior. *Mol Psychiatry* 14(7):719–727.
37. Balu DT, Lucki I (2009) Adult hippocampal neurogenesis: Regulation, functional implications, and contribution to disease pathology. *Neurosci Biobehav Rev* 33(3): 232–252.
38. Li Y, Krupa B, Kang JS, Bolshakov VY, Liu G (2009) Glycine site of NMDA receptor serves as a spatiotemporal detector of synaptic activity patterns. *J Neurophysiol* 102(1):578–589.
39. Townsend M, Yoshii A, Mishina M, Constantine-Paton M (2003) Developmental loss of miniature N-methyl-D-aspartate receptor currents in NR2A knockout mice. *Proc Natl Acad Sci USA* 100(3):1340–1345.
40. Cull-Candy SG, Leszkiewicz DN (2004) Role of distinct NMDA receptor subtypes at central synapses. *Sci STKE* 2004(255):re16.
41. Zucker RS, Regehr WG (2002) Short-term synaptic plasticity. *Annu Rev Physiol* 64: 355–405.
42. Balu DT, Coyle JT (2012) Neuronal D-serine regulates dendritic architecture in the somatosensory cortex. *Neurosci Lett* 517(2):77–81.
43. DeVito LM, et al. (2011) Serine racemase deletion disrupts memory for order and alters cortical dendritic morphology. *Genes Brain Behav* 10(2):210–222.
44. Vo N, et al. (2005) A cAMP-response element binding protein-induced microRNA regulates neuronal morphogenesis. *Proc Natl Acad Sci USA* 102(45):16426–16431.
45. Mellios N, et al. (2011) miR-132, an experience-dependent microRNA, is essential for visual cortex plasticity. *Nat Neurosci* 14(10):1240–1242.
46. Zhou Z, et al. (2006) Brain-specific phosphorylation of MeCP2 regulates activity-dependent Bdnf transcription, dendritic growth, and spine maturation. *Neuron* 52(2): 255–269.
47. Klein ME, et al. (2007) Homeostatic regulation of MeCP2 expression by a CREB-induced microRNA. *Nat Neurosci* 10(12):1513–1514.
48. Orozco-Ibarra M, et al. (2007) Evaluation of oxidative stress in D-serine induced nephrotoxicity. *Toxicology* 229(1–2):123–135.
49. Phillips RG, LeDoux JE (1992) Differential contribution of amygdala and hippocampus to cued and contextual fear conditioning. *Behav Neurosci* 106(2):274–285.
50. Chowdhury N, Quinn JJ, Fanselow MS (2005) Dorsal hippocampus involvement in trace fear conditioning with long, but not short, trace intervals in mice. *Behav Neurosci* 119(5):1396–1402.
51. Misane I, et al. (2005) Time-dependent involvement of the dorsal hippocampus in trace fear conditioning in mice. *Hippocampus* 15(4):418–426.
52. Quinn JJ, Loya F, Ma QD, Fanselow MS (2005) Dorsal hippocampus NMDA receptors differentially mediate trace and contextual fear conditioning. *Hippocampus* 15(5): 665–674.
53. McEchron MD, Bouwmeester H, Tseng W, Weiss C, Disterhoft JF (1998) Hippocampectomy disrupts auditory trace fear conditioning and contextual fear conditioning in the rat. *Hippocampus* 8(6):638–646.
54. Papouin T, et al. (2012) Synaptic and extrasynaptic NMDA receptors are gated by different endogenous coagonists. *Cell* 150(3):633–646.
55. Li Y, et al. (2013) Identity of enodgenous NMDAR glycine site agonist in amygdala is determined by synaptic activity level. *Nat Commun* 4:1760.
56. Coultrap SJ, Nixon KM, Alvestad RM, Valenzuela CF, Browning MD (2005) Differential expression of NMDA receptor subunits and splice variants among the CA1, CA3 and dentate gyrus of the adult rat. *Brain Res Mol Brain Res* 135(1-2):104–111.
57. Morris RG, Anderson E, Lynch GS, Baudry M (1986) Selective impairment of learning and blockade of long-term potentiation by an N-methyl-D-aspartate receptor antagonist, AP5. *Nature* 319(6056):774–776.
58. Hill JJ, et al. (2005) Analysis of pyramidal neuron morphology in an inducible knockout of brain-derived neurotrophic factor. *Biol Psychiatry* 57(8):932–934.
59. Hong EJ, McCord AE, Greenberg ME (2008) A biological function for the neuronal activity-dependent component of Bdnf transcription in the development of cortical inhibition. *Neuron* 60(4):610–624.
60. Impey S, et al. (2004) Defining the CREB regulon: A genome-wide analysis of transcription factor regulatory regions. *Cell* 119(7):1041–1054.
61. Im HI, Hollander JA, Bali P, Kenny PJ (2010) MeCP2 controls BDNF expression and cocaine intake through homeostatic interactions with microRNA-212. *Nat Neurosci* 13(9):1120–1127.
62. Tanaka J, et al. (2008) Protein synthesis and neurotrophin-dependent structural plasticity of single dendritic spines. *Science* 319(5870):1683–1687.
63. Li N, et al. (2010) mTOR-dependent synapse formation underlies the rapid antidepressant effects of NMDA antagonists. *Science* 329(5994):959–964.
64. Jaworski J, Spangler S, Seeburg DP, Hoogenraad CC, Sheng M (2005) Control of dendritic arborization by the phosphoinositide-3′-kinase-Akt-mammalian target of rapamycin pathway. *J Neurosci* 25(49):11300–11312.
65. Ryazanov AG, Shestakova EA, Natapov PG (1988) Phosphorylation of elongation factor 2 by EF-2 kinase affects rate of translation. *Nature* 334(6178):170–173.
66. Scheetz AJ, Nairn AC, Constantine-Paton M (2000) NMDA receptor-mediated control of protein synthesis at developing synapses. *Nat Neurosci* 3(3):211–216.
67. Sutton MA, Taylor AM, Ito HT, Pham A, Schuman EM (2007) Postsynaptic decoding of neural activity: eEF2 as a biochemical sensor coupling miniature synaptic transmission to local protein synthesis. *Neuron* 55(4):648–661.
68. Verpelli C, et al. (2010) Synaptic activity controls dendritic spine morphology by modulating eEF2-dependent BDNF synthesis. *J Neurosci* 30(17):5830–5842.
69. Emamian ES (2012) AKT/GSK3 signaling pathway and schizophrenia. *Front Mol Neurosci* 5:33.
70. Lai WS, et al. (2006) Akt1 deficiency affects neuronal morphology and predisposes to abnormalities in prefrontal cortex functioning. *Proc Natl Acad Sci USA* 103(45): 16906–16911.
71. Coyle JT, Basu A, Benneyworth M, Balu D, Konopaske G (2012) Glutamatergic synaptic dysregulation in schizophrenia: Therapeutic implications. *Handbook Exp Pharmacol* 213:267–295.
72. Tsai GE, Lin PY (2010) Strategies to enhance N-methyl-D-aspartate receptor-mediated neurotransmission in schizophrenia, a critical review and meta-analysis. *Curr Pharm Des* 16(5):522–537.
73. Benneyworth MA, Coyle JT (2012) Altered acquisition and extinction of amphetamine-paired context conditioning in genetic mouse models of altered NMDA receptor function. *Neuropsychopharmacology* 37(11):2496–2504.
74. Dahl D, Burgard EC, Sarvey JM (1990) NMDA receptor antagonists reduce medial, but not lateral, perforant path-evoked EPSPs in dentate gyrus of rat hippocampal slice. *Exp Brain Res* 83(1):172–177.
75. Steward O (1976) Topographic organization of the projections from the entorhinal area to the hippocampal formation of the rat. *J Comp Neurol* 167(3):285–314.
76. Shin RM, Tsvetkov E, Bolshakov VY (2006) Spatiotemporal asymmetry of associative synaptic plasticity in fear conditioning pathways. *Neuron* 52(5):883–896.
77. Tsvetkov E, Carlezon WA, Benes FM, Kandel ER, Bolshakov VY (2002) Fear conditioning occludes LTP-induced presynaptic enhancement of synaptic transmission in the cortical pathway to the lateral amygdala. *Neuron* 34(2):289–300.
78. Balu DT, Basu AC, Corradi JP, Cacace AM, Coyle JT (2012) The NMDA receptor co-agonists, D-serine and glycine, regulate neuronal dendritic architecture in the somatosensory cortex. *Neurobiol Dis* 45(2):671–682.
79. Paxinos G, Franklin KBJ (2001) *The Mouse Brain in Stereotactic Coordinates* (Academic Press, San Diego), 2nd Ed.
80. Wibrand K, et al. (2010) Differential regulation of mature and precursor microRNA expression by NMDA and metabotropic glutamate receptor activation during LTP in the adult dentate gyrus in vivo. *Eur J Neurosci* 31(4):636–645.
81. Balu DT, Coyle JT (2011) Glutamate receptor composition of the post-synaptic density is altered in genetic mouse models of NMDA receptor hypo- and hyperfunction. *Brain Res* 1392:1–7.
82. Hashimoto A, Nishikawa T, Oka T, Takahashi K, Hayashi T (1992) Determination of free amino acid enantiomers in rat brain and serum by high-performance liquid chromatography after derivatization with N-tert.-butyloxycarbonyl-L-cysteine and o-phthaldialdehyde. *J Chromatogr A* 582(1–2):41–48.

Supporting Information

Balu et al. 10.1073/pnas.1304308110

Materials and Methods

Subcellular Fractionation. Tissue was homogenized in a glass-glass potter in 0.4 mL of ice-cold 0.32 M sucrose containing 20 mM Hepes (pH = 7.4), 1 mM EDTA, 10 μg/mL aprotinin, 0.5 μg/mL antipain, 0.1 μg/mL pepstatin A, and 1 mM phenylmethanesulfonyl fluoride (Sigma Alrdich), as well as phosphatase inhibitors [mixtures A and B, 1% (vol/vol); Santa Cruz Biotechnology]. A 60-μL aliquot was reserved, sonicated, and stored at −80 °C. This aliquot served as the whole-cell lysate fraction. The resultant of homogenized tissue was centrifuged at 1,011 × *g* for 10 min at 4 °C to separate a pellet enriched in nuclear components and large cellular debris from the supernatant (S1). Next, 100 μL of sucrose buffer was added to the nuclear pellet. The pellet was sonicated and centrifuged at 16,181 × *g* for 5 min at 4 °C to remove insoluble debris. S1 was centrifuged at 16,181 × *g* for 10 min at 4 °C to obtain the cytosolic fraction (S2). The pellet (crude synaptosomal fraction) was resuspended and sonicated in tissue lysis buffer [60 mM Tris (pH 6.8), 2% SDS, and the same protease and phosphatase inhibitors as mentioned above]. Protein concentrations were measured using the Bradford protein assay (Bio-Rad).

Western Blot Analysis. Samples were lysed in the same buffer used for the BDNF ELISA. Samples (20 μg protein) were electrophoretically separated on an SDS polyacrylamide gel (7.5–12%). The phospho-protein was immunoblotted first, after which the membrane was stripped, washed, reblocked, and incubated with the total protein primary antibody. Semiquantitative assessment of protein bands was performed by measuring chemiluminescent signal using a ChemiDoc XRS Imager and Image Lab 4.0 Software (Bio-Rad).

Immunoprecipitation. A separate cohort of mice from the ELISA and Western blot analyses was used for immunoprecipitation. 2 μg of rabbit polyclonal anti-TrkB antibody (Abcam) was added to tissue lysate containing 10 mg of tissue and rotated at 4 °C for 3 h. Immunoprecipitation was carried out using the Dynabeads Protein G Immunoprecipitation kit (Invitrogen). The supernatant was removed, the tissue lysate-TrkB (tropomyosin receptor kinase B) antibody solution was added to 50 μL of Dynabeads, and the tubes were rotated at 4 °C overnight. The beads were washed according to the manufacturer's protocol. SDS/PAGE and immunoblotting was performed as described above. TrkB phosphorylation was measured by immunoblotting for phosphotyrosine, stripping the membrane, and then reprobing for TrkB. pTyr OD values (average of two bands) were divided by their corresponding TrkB OD values (average of two bands). The mutant values were normalized to WT values (percent control) collected in parallel from the same gel. The normalized values were then averaged and used for statistical analysis.

HPLC Analysis of D-Serine. Amino acids were derivatized using *o*-phthaldialdehyde (Alfa Aesar) and *N*-tert-butyloxycarbonyl-L-cysteine (Novabiochem). Amino acid peaks were resolved using a binary gradient of 25 mM sodium acetate (pH 6.5) and acetonitrile. The gradient progressed from 10 to 20% acetonitrile over the course of 25 min. Amino acid concentrations (μmol/g) were calculated by comparing an internal standard, L-homocysteic acid (L-HCA), to standard samples run at the beginning of each analysis using the following formula: (Peak height of L-HCA in standard sample/Peak height of D-serine in standard sample) × (Peak height of D-serine in tissue sample/Peak height of L-HCA in tissue sample) × [Amount of L-HCA in tissue sample (μmol)/Amount of tissue (g)]. Serum samples were treated identically to brain tissue samples.

Assessment of Kidney Tubular Integrity. Kidneys were removed from chronically treated WT and serine racemase-null mutant ($SR^{-/-}$) mice (n = 2/genotype) and placed in ice-cold 4% paraformaldehyde solution. Paraffin embedding, sectioning, hematoxylin and eosin staining was performed by the Rodent Histopathology Core Facility of the Dana-Farber/Harvard Cancer Center (P30 CA06516).

Trace Fear Conditioning. On day 1, each conditioning session consisted of a 3-min acclimation period followed by seven trials of the following structure: a 20-s tone at 75 dB followed by a 20-s trace period followed by a mild footshock (duration 2 s, amplitude 0.7 mA). Trials were roughly 4 min apart. On day 2, mice were placed in the same conditioning chambers as on day 1 and freezing behavior was measured for 8 min. On day 3, mice were placed in chambers with different contextual cues, including a smooth chamber floor, a peppermint odor (peppermint extract diluted 1:1 K), and a roof insert to distinguish the testing environment from the conditioning environment. The protocol from day 1 was repeated without the footshock. The house light in the chamber was illuminated during all sessions.

Hot-Plate Test. The mice were placed into a glass cylinder on a hot plate adjusted to 52 °C (Bioseb). Two trials separated with 5–10 min interval were carried out. For the first trial, the latency of the first reaction (licking, flinches, little leaps) was recorded, with a maximum of 30 s. For the second trial, in addition to the first reaction, the latency to jump was also recorded. A 3-min cutoff was used for the second trial.

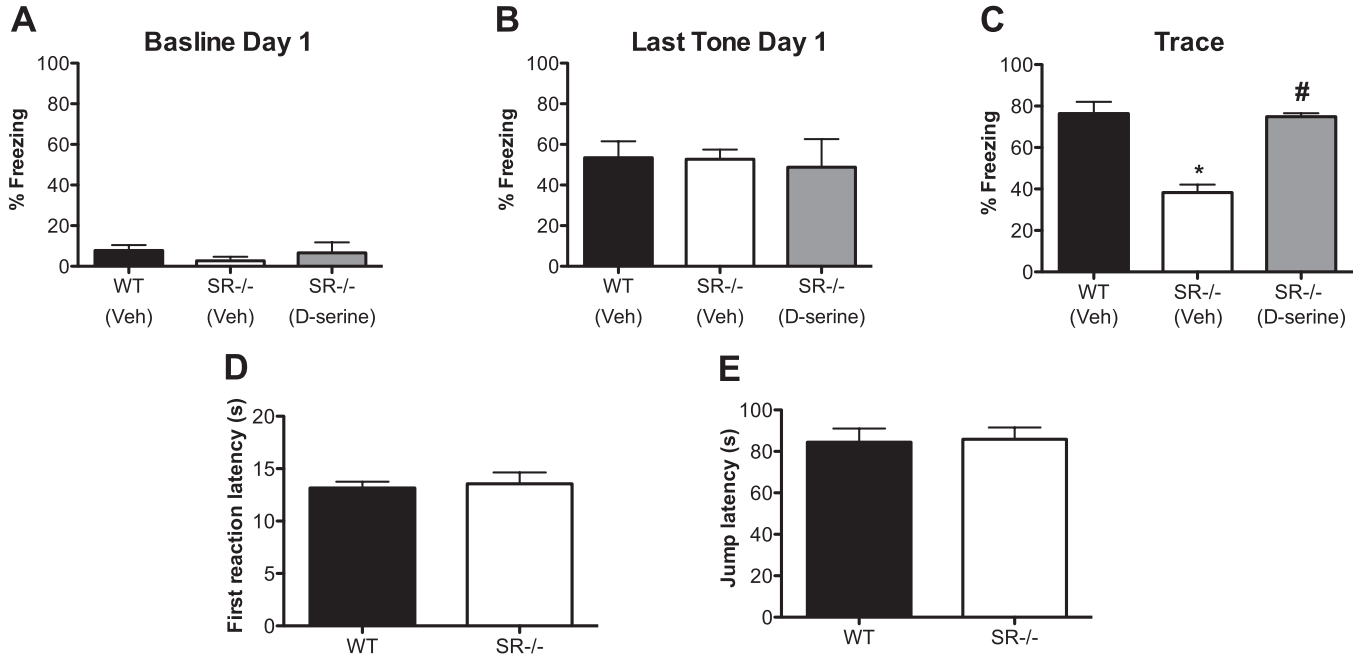

Fig. S1. Baseline freezing and pain sensitivity is unaltered in $SR^{-/-}$ mice. (*A*) WT ($n = 11$; black bars), $SR^{-/-}$ ($n = 5$; white bars), and $SR^{-/-}$ mice treated with D-serine ($n = 5$; gray bars) equally ($P > 0.05$) displayed very little nonassociative freezing during the 3-min acclimation period on day 1. (*B*) There was no significant difference in freezing behavior among groups across the seven tone presentations on day 1 [repeated-measures ANOVA; genotype: $F(2, 114) = 1.88$, $P = 0.2$] with all groups freezing equally by the last tone. (*C*) $SR^{-/-}$ mice froze less during the 20-s trace intervals (average freezing during each interval) on day 3, a deficit that was reversed by chronic D-serine treatment [$F(2,9) = 13.17$, $P < 0.005$; *, different from WT; #, different from SR−/− vehicle]. There was no difference between WT ($n = 12$) and $SR^{-/-}$ ($n = 12$) mice in thermal pain sensitivity in the hot plate assay, as measured by the latency of the first reaction (*D*; licking, flinches, little leaps) and (*E*) the latency to jump. All values represent the mean ± SEM.

Table S1. $SR^{-/-}$ mice exhibit many of the structural, neurochemical, and cognitive abnormalities that are observed in schizophrenia

Structural, molecular, and functional brain changes	Schizophrenia	$SR^{-/-}$
Reduced dendritic complexity	✓	✓
Reduced spine density	✓	✓
Cortical/hippocampal atrophy	✓	✓
Reduced BDNF/TrkB/Akt signaling	✓	✓
Reduced microRNA-132	✓	✓
Subtle cognitive impairments	✓	✓

Table S2. Primers used for quantitative PCR analyses

Gene	Source	Primer
GAPDH	Applied Biosystems	Mm99999915_g1
BDNF	Applied Biosystems	Mm04230607_s1
pri-miR-132	Applied Biosystems	Mm03306275_pri
premiR-132	N/A	5′ CGA CCA TGG CTG TAG ACT GTT 3
miR-16	N/A	5′ CCT GTC ACA CTA AAG CAG CA 3′
miR-132	Applied Biosystems	000457
snoRNA202	Applied Biosystems	001232
premiR-132	N/A	Forward: 5′AAC CGT GGC TTT CGA TTG TTA 3′
	N/A	Reverse: 5′CGA CCA TGG CTG TAG ACT GTT 3′
miR-16	N/A	Forward: 5′CCG CTC TAG CAG CAC GTA A 3′
	N/A	Reverse: 5′CCT GTC ACA CTA AAG CAG CA 3′

Table S3. Antibodies used for Western blot analyses

Antibody	Dilution	Supplier	Catalog No.
Primary			
Akt	1:1,000	Cell Signaling	9272
Akt1	1:1,000	Cell Signaling	2938
-actin	1:8,000	Abcam	8229
CREB	1:1,000	Cell Signaling	9197
eEF2	1:1,000	Cell Signaling	2332
Erk1/2	1:1,000	Cell Signaling	9102
GSK3a/b	1:1,000	Cell Signaling	5676
MeCP2	1:1,000	Millipore	07–013
MEK-1/2	1:1,000	Santa Cruz	sc-81504
mTOR	1:2,000	Millipore	07–231
p70 S6 kinase	1:1,000	Cell Signaling	2708
phospho-4E-BP-1 (Thr37/46)	1:1,000	Cell Signaling	2855
phospho-Akt (Ser473)	1:1,000	Cell Signaling	4058
phospho-Akt (Thr308)	1:1,000	Cell Signaling	4056
phospho-Akt1 (Ser473)	1:1,000	Cell Signaling	9018
phospho-CREB (Ser133)	1:1,000	Cell Signaling	9196
phospho-GSK3a/b (Ser21/9)	1:1,000	Cell Signaling	8566
phospho-eEF2 (Thr56)	1:1,000	Cell Signaling	2331
phospho-Erk1/2 (Thr202/Tyr204)	1:1,000	Cell Signaling	9101
phospho-MEK-1/2 (Ser218/Ser222)	1:1,000	Santa Cruz	sc-7995
phospho-p70 S6 kinase (Thr389)	1:1,000	Cell Signaling	9205
phosphotyrosine (pY99)	1:4,000	Santa Cruz	sc-7020
TrkB	1:1,000	BD Transduction	610101
TrkB (used for IP)	2 g	Abcam	ab33655
Secondary			
Goat anti-rabbit	1:5,000	Abcam	ab6721
Rabbit anti-mouse	1:3,000	Abcam	ab6728

CREB, cyclic AMP-responsive element binding; eEF2, eukaryotic elongation factor 2; GSK3, glycogen synthase kinase 3; MeCP2, Methyl CpG binding protein 2; mTOR, mammalian target of rapamycin; phospho-4E-BP-1, eukaryotic translation initiation factor 4E-binding protein 1; TrkB, tropomyosin receptor kinase B.